small
NANO MICRO

Water-Dependent Photonic Bandgap in Silica Artificial Opals

Francisco Gallego-Gómez, Alvaro Blanco, Victor Canalejas-Tejero, and Cefe López*

Some characteristics of silica-based structures—like the photonic properties of artificial opals formed by silica spheres—can be greatly affected by the presence of adsorbed water. The reversible modification of the water content of an opal is investigated here by moderate heating (below 300 °C) and measuring in situ the changes in the photonic bandgap. Due to reversible removal of interstitial water, large blueshifts of 30 nm and a bandgap narrowing of 7% are observed. The latter is particularly surprising, because water desorption increases the refractive index contrast, which should lead instead to bandgap broadening. A quantitative explanation of this experiment is provided using a simple model for water distribution in the opal that assumes a nonclose-packed fcc structure. This model further predicts that, at room temperature, about 50% of the interstitial water forms necks between nearest-neighbor spheres, which are separated by 5% of their diameter. Upon heating, dehydration predominantly occurs at the sphere surfaces (in the opal voids), so that above 65 °C the remaining water resides exclusively in the necks. A near-close-packed fcc arrangement is only achieved above 200 °C. The high sensitivity to water changes exhibited by silica opals, even under gentle heating of few degrees, must be taken into account for practical applications. Remarkably, accurate control of the distance between spheres—from 16 to 1 nm—is obtained with temperature. In this study, novel use of the optical properties of the opal is made to infer quantitative information about water distribution within silica beads and dehydration phenomena from simple reflection spectra. Taking advantage of the well-defined opal morphology, this approach offers a simple tool for the straightforward investigation of generic adsorption–desorption phenomena, which might be extrapolated to many other fields involving capillary condensation.

1. Introduction

3D photonic crystals (PhCs) are interesting optical materials for the accurate control of light propagation in all directions. These structures can exhibit a complete photonic bandgap (PBG), in which light of a certain energy range cannot propagate. Artificial opals, consisting of solid colloidal crystals of self-assembled spheres, have been widely employed as inexpensive and versatile PhCs.[1] Opals made of submicrometer spheres of amorphous SiO_2 in a face-centered cubic (fcc) packing arrangement are particularly easy-to-fabricate structures displaying PhC properties.[2] These properties (position, width, and reflectance/transmittance of the PBG) are directly related to the size and packing of the spheres, but also to the refractive indices involved in the opal, i.e., the silica of the spheres and the surrounding medium (generally air).

Due to the amphiphilic character of amorphous silica, water from the surrounding moisture is expected to be adsorbed onto a sphere's surface through hydrogen bonds

Dr. F. Gallego-Gómez, Dr. A. Blanco, V. Canalejas-Tejero, Dr. C. López
Instituto de Ciencia de Materiales de Madrid
and Unidad Asociada CSIC-UVigo
c/Sor Juana Inés de la Cruz 3, 28049 Madrid, Spain
E-mail: francisco.gallego@icmm.csic.es

DOI: 10.1002/smll.201100184

NANO MICRO small

to silanol groups, staying in the opal interstices (interstitial water). Although the amount of adsorbed water can be important and might significantly affect the opal photonic properties, this has been barely considered.[3–6] Moreover, most of the few studies related to this issue focus on the influence of the removal of water from inside the silica spheres (internal water structurally trapped within the spheres during their synthesis). Thereby, the content of water in silica opals is permanently reduced by long-lasting thermal annealing up to 1100 °C and the optical properties, measured after (and not during) water loss, are irreversibly modified. Thus, there are no studies on the reversible de/rehydration of interstitial water in silica opals (by, e.g., restrained annealing) and its influence in situ on the optical properties. The amount of water in silica opals significantly varies upon moderate alteration of the surrounding conditions like temperature (T), humidity, or pressure. This makes it necessary to know the reach of such changes in a changable environment (e.g., inside a warming optoelectronic housing). These features offer, in turn, a straightforward tool for the reversible tuning of PhCs by accurately modifying the amount of water in the opal.

Here we show large and reversible changes of the photonic bandgap properties by means of controlled water evaporation and re-adsorption in as-grown silica opals. To analyze and simulate the opal structure, we use accurate calculations based on the plane-wave expansion method.[7] This method, in contrast to others like the Korringer–Kohn–Rostoker[8] or the scalar-wave[9] approximations, allows the computation of the photonic gaps in heterogeneous periodic structures (in our case, formed by silica, air, and water) having a nonuniform distribution. From the water content (measured by thermogravimetric analysis, TGA) and the experimental T-dependence of the PBG, a simple model is used to infer where water is located in the opal as well as its evolution upon evaporation.

2. Results and Discussion

2.1. Temperature-Dependent Water Content in the Opal

TGA monitors the removal of both internal and interstitial water from the silica opal. **Figure 1** shows an accumulated weight loss in the opal of 11.8 wt.% until 850 °C. A pronounced loss of 7.5 wt.% occurs during heating up to ~100 °C, followed by a plateau up to ~210 °C and further removal of 4.3 wt.% up to ~700 °C, where it levels off. The abrupt drop-off (region I in Figure 1, inset) corresponds to the desorption of weakly bonded interstitial water.[10,11] After the plateau (region II), the weight loss is associated to desorption of residual (more strongly bonded) interstitial water due to surface dehydroxilation (region III). Above ~400 °C (region IV), irreversible condensation of silanol groups occurs,[11] while the internal water from the silica spheres (about 2 wt.% of the total) is removed at temperatures above 500–600 °C.[4,10,11] This removal is accompanied by shrinkage of the silica spheres at $T > 750$ °C, as demonstrated by scanning electron microscopy analysis in reference [4]. According to this, the silica opal contains

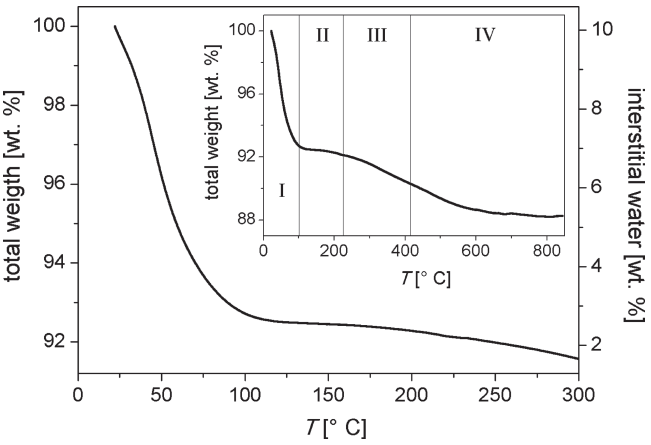

Figure 1. TGA of an as-grown silica opal. Inset shows the whole temperature range measured. The amount of interstitial water is represented at the right axis.

about 10 wt.% of interstitial water, most of which (~7 wt.%) is rapidly removed below 100 °C, while an important remnant (~2 wt.%) requires heating above 300 °C (right axis in Figure 1). These quantities are consistent with previous studies on silica spheres, performed either as nonassembled beads[4,10,11] or in opal structures.[3,5]

Irreversible changes in the silica spheres can be then ruled out below 400 °C. Reversible thermal processes in regions I–III are predominantly attributed to interstitial water. Other reversible phenomena affecting the spheres' internal water can eventually occur, like water exchange between internal reservoirs and lattice interstices, with subsequent sphere size and/or refractive index changes. However, it has been shown that silica spheres' outermost volume is almost poreless and reversible liquid exchange, if any, occurs very slowly (over many hours).[4] From these considerations, we assume that heating below 400 °C (regions I–III) only affects the content of adsorbed water on the spheres surface (i.e., interstitial water in the opal), and that in a reversible way. If the heating temperature is restricted to those regions, the morphology (size and form) and physical properties (refractive index and density) of the silica spheres are not affected, which strongly simplifies the analysis. A drawback of such restriction in the heating temperature is that the interstitial water cannot be completely removed, so some amount of adsorbed water will always be present. In the following we investigate the changes induced in the opal structure by controlled heating below 300 °C and analyze them as function of the T-dependent water content (as obtained from Figure 1). Hereafter we only refer to interstitial water.

2.2. Water-Dependent PBG Changes: Deviations from Ideal FCC Structure

The increase of the opal temperature has an immediate effect on its optical properties as water is removed. This is demonstrated by heating the opal (from room temperature, RT, to 285 °C) and measuring its reflectance in situ (**Figure 2**a). Upon heating, the Bragg peak shows a

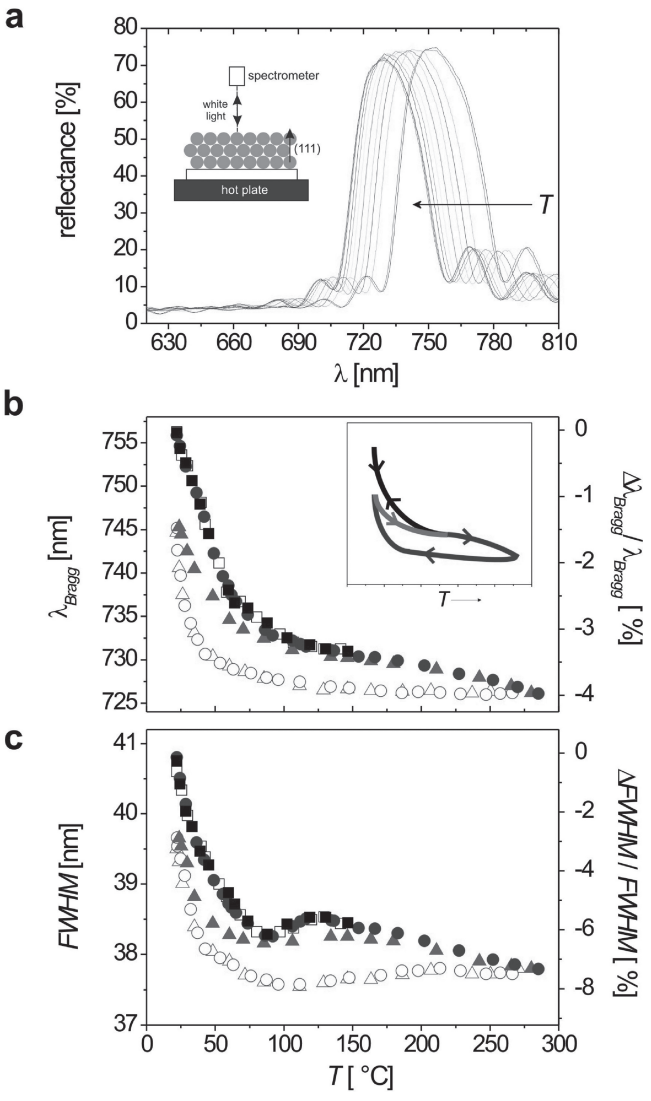

Figure 2. a) Change of the opal reflection spectrum upon heating from RT to 285 °C. Inset: scheme of the experimental setup, where the silica opal is placed on a hot plate while reflection spectra are simultaneously recorded. b) Experimental evolution of λ_{Bragg} and c) of FWHM upon several heating and cooling cycles (solid and empty symbols, respectively). The heating/cooling/heating cycle between RT and 150 °C (black squares and dark grey solid circles) shows complete reversibility without hysteresis, while the cycles between RT and 285 °C (dark grey circles and light grey triangles) shows partial irreversibility and pronounced hysteresis. Following hysteresis cycles are fully reproducible. Inset in (b) schematizes the observed behavior: changes upon heating up to 150 °C are completely reversible without hysteresis (black line); above 150 °C (up to 285 °C), changes are mostly but not completely reversible, and show pronounced hysteresis (dark and light grey lines; arrows represent undefined number of cycles).

marked blueshift while the reflectance slightly decreases. The *T*-dependence (Figures 2b,c) of the PBG position (λ_{Bragg}) and width (given by the full-width half-maximum, FWHM) closely resembles that measured by TGA in Figure 1, which evidences their strong correlation with the water content in the opal. The PBG shifts about 22 nm to shorter wavelengths during heating to 100 °C (which corresponds to region I in Figure 1), followed by a plateau (region II) and a further blueshift above 200 °C (in region III) up to an overall shift of –30 nm at 285 °C. The Bragg peak clearly narrows during heating, although some broadening in region II, with an overall FWHM decrease of ~7%. It is remarkable the large response of the PBG to slight heating above RT, which shows, e.g., a blueshift as large as 6 nm by increasing *T* only 10 °C. This is obviously related to the abrupt water desorption observed in Figure 1 right above RT and demonstrates the high sensitivity of the PhC properties of a silica opal to varying ambient conditions.

The observed changes are essentially reversible and the Bragg peak tends to its original form and position upon cooling (Figures 2b,c). However, two regimes must be distinguished. Changes induced by heating up to ~150 °C are fully reversible and the PBG evolution upon cooling perfectly matches that upon heating (no hysteresis). On the contrary, heating above 150 °C provokes partially irreversible changes in the PBG and a clear hysteresis loop is observed. In both regimes, PBG changes are fully reproducible by repeated heating/cooling cycles (as sketched in Figure 2b, inset). Such repeatability supports that no permanent modifications were significantly induced in the spheres by annealing under these conditions. It is worth noting that the slight irreversibility observed in Figure 2 (1.7% of λ_{Bragg}) agrees with the results reported by Miguez et al., in which some permanent change (about 2% of λ_{Bragg}) is measured after opal annealing at 200 °C (while no changes were observed after 100 °C-annealing).[3] Since irreversibility is accompanied by hysteresis and both are currently encountered in adsorption–desorption experiments at mesoporous systems (usually associated to metastability in capillary condensation,[11,12] we suggest that the opal ceases to fully re-adsorb the desorbed water. However, other possibilities could also be considered. For example, syneresis (condensation by ageing),[13] which is typically favored in the presence of an aqueous medium and by increasing temperatures, could cause spheres shrinkage. However, the observation of shrinkage in silica spheres only at $T > 750$ °C[4] suggests that this effect is improbable at $T < 300$ °C. Lattice rearrangement leading to some permanent distortion of the fcc structure could also explain some irreversible blueshift of λ_{Bragg}. Eventually, this could be discerned by simultaneous analysis of the high-energy photonic resonances of the opal.[14]

Are the experimental data compatible with an ideal (close-packed) fcc opal structure? In this case, the nearest-neighbor beads are in contact and the adsorbed water is only placed in the opal voids. Water desorption only implies the decrease of n_v (the refractive index of the interstitial void region, see Experimental Section, Equation 2) since the opal structure remains unchanged (lattice parameter d_{111} and filling factor *f* are constant). Qualitatively, the Bragg peak is indeed expected to blueshift on heating caused by the subsequent decrease of the effective refractive index n_{eff} and, thus, of λ_{Bragg} (Experimental Section, Equation 1). However, the reduction of n_v means a higher refractive index contrast in the opal, which would lead to a broader bandgap.[15] This prediction is clearly contradicted by the experimental FWHM. Quantitatively, further important discrepancies are found, as discussed in the next section.

NANO MICRO small

On the contrary, if we consider a nonclose fcc packing, beads are not in mechanical contact and the adsorbed water is not only placed in the voids but also between adjacent spheres. Thus, water desorption not only leads to an n_v decrease but also to the compaction of the structure, which means both the contraction of d_{111} and the increase of f. This new scenario drastically modifies the water-dependence of the opal properties as follows. On the one hand, a larger PBG blueshift would be now expected upon heating due to the additional contribution of the decreasing d_{111}, as λ_{Bragg} linearly depends on d_{111} (Equation 1). The simultaneous increase of f contributes with the opposite sign (to some PBG redshift), but sublinearly (Equation 1). On the other hand, regarding the PBG width, the increase of f leads to a reduction of the scattering strength and, accordingly, to gap narrowing.[15] This contribution can eventually overcome that due to the n_v decrease, which would explain the measured FWHM behavior.

2.3. Model Versus Experiment: Close-Packed and Nonclose-Packed FCC Structure

Quantitative analysis of the implications of these features was then attempted by modeling the opaline silica/water/air structure in a simple way. Although nonclose fcc packing in artificial opals has been previously suggested,[3,16] here we quantify the discrepancies with the close-packed case, including, the effect of adsorbed water. The nonclose packing is demonstrated to be a natural scenario explaining the experiments without further assumptions: the nonclose-packed structure would be a direct consequence of the presence of adsorbed water between the spheres and, in turn, water desorption gives experimental proof for that.

As a premise, we only consider isotropic fcc structures formed by perfect spheres, independently of the close or nonclose packing. Disorder effects are excluded, which is justified by the high opal reflectance (close to 80%). Moreover, the unchanged reflectance upon heating (Figure 2a) suggests that the defects in the opal remain practically unaffected during measurements. A simple model is assumed for the water distribution in the opal, distinguishing between water placed in the opal voids, building a film up on the silica surface, and water between adjacent spheres, forming necks (**Scheme 1**, top). To quantify the latter attribute, we define the parameter ρ as the ratio of water in the necks to the total water.

For quantitative simulations we describe the water neck as a biconcave disk of radius R, the faces of which are delimited by the two nearest neighbor spheres. The width at its center, η, gives the distance between the spheres (see Scheme 1, bottom), which is distinctive for the nonclose-packed fcc case (i.e., only $\eta = 0$ corresponds to the close packing). The water film in the voids is accepted to have a homogeneous thickness d. Thus, assuming only the sphere diameter (D), the opal is fully characterized in our model by three geometric parameters: d, R, and η (the ratio ρ is just a function of them). If they are known, the amount of water is easily obtained from the volume ratio of both film and neck to the silica spheres in a fcc unit cell determined by ($D + \eta$) instead of D. In turn, if the water content is known, e.g., from TGA as

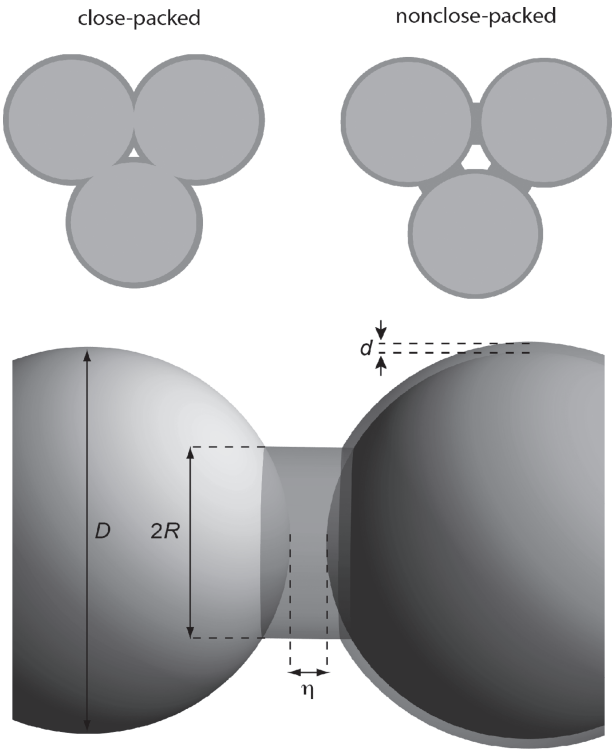

Scheme 1. Sketch of the distribution patterns of the interstitial water in the opal. Top left: close-packed fcc case ($\eta = 0$); top right: nonclose-packed fcc case ($\eta \neq 0$). Bottom: model for the water distribution in the opal (see text for details).

in our case, a number of terns {d, η, R} are compatible. Since each of them yields different PBG properties, they can be compared with the experimental data in order to discern the more realistic water distribution pattern. On this basis, we can easily explore the bandgap behavior expected for different configurations as a function of the water content, which is the essential parameter in our experiment.

To allow a direct comparison, we plot in **Figure 3** the measured data (first heating cycle up to 285 °C from Figures 2b,c) against the amount of water by using the correspondence with T obtained from TGA. The bottom axis represents decreasing water content up to ~1.8 wt.%, which is the change direction in our heating experiment (see T in top axis). As discussed above, we do not consider removing water towards 0 wt.%, which requires temperatures affecting the silica spheres, so that our model ceases to be valid. Experimentally, both λ_{Bragg} and FWHM show a nearly linear dependence with water content up to ~2.7 wt.% (T ~ 100 °C, which corresponds to region I in Figure 1), while they change more pronouncedly at less water content, i.e., at higher T (regions II and III). This reflects the fact that the bandgap still varies significantly above 100 °C in spite of the small loss of water. According to our model and using MPB (see Experimental Section), we simulate the PBG properties for both close and nonclose cases and compare with the experiment:

Close-Packed FCC ($\eta = 0$): In this case both the thickness d of the water film and the neck radius R, related by the amount of water, need to be determined. That is, a number of configurations {d, 0, R} are compatible with the water content.

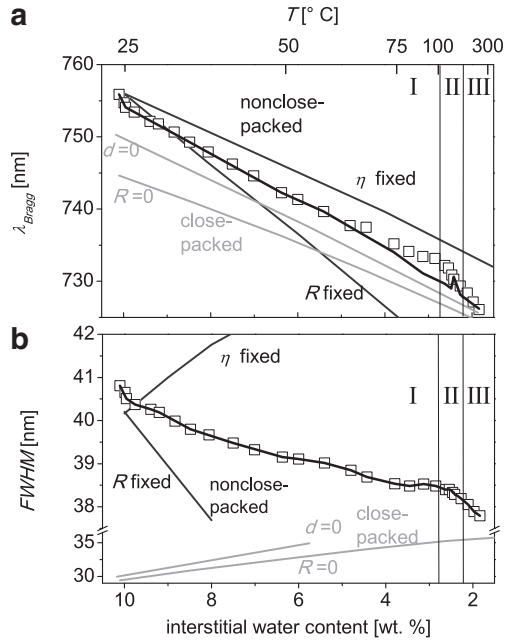

Figure 3. Comparison between experimental (symbols) and theoretical (lines) evolution of λ_{Bragg} (a) and FWHM (b) for progressive loss of interstitial water. Gray lines correspond to MPB calculations for close-packed fcc (light gray lines), for fixed $d = 0$ nm and fixed $R = 0$ nm, and for nonclose-packed fcc case (with constant ratio ρ, dark gray lines), for fixed $\eta = 16$ nm and fixed $R = 70$ nm. Solid black lines correspond to the best fit obtained with adjustable parameters d, η, and R. Regions I–III as identified in Figure 1 are also included.

In order to cover the limit cases, we simulate the behavior, on the one hand, for $R = 0$ nm (no water necks) and d variable, and, on the other hand, for $d = 0$ nm (no water layer on the spheres) and changing R (Figure 3). Unfortunately, both limits (qualitatively similar) show a dramatic disagreement with the experiment. In particular, the mismatch with FWHM at RT is 14 nm (about one-third). Even more importantly, the PBG is predicted to broaden with decreasing water content, which obviously contradicts the measurement. Further, the PBG is predicted to blueshift, like in the experiment, but ~13 nm less, almost half of the measured change.[17]

Nonclose-Packed FCC ($\eta \neq 0$): Now, a number of configurations $\{d, \eta, R\}$ are possible for each water content. In particular for 10.1 wt.%, the choice (without further adjustment) of $d = 5$ nm, $\eta = 14$ nm and $R = 73$ nm (which correspond to $\rho = 0.699$) provides a good accord between theoretical and experimental PBGs (Figure 3). The simulation of the subsequent loss of water requires, again, some assumption. For simplicity, we assume that both film and water neck diminish equally (i.e., ρ is constant). Then, in order to simulate how the neck diminishes, it is illustrative to consider two limits: a) η is kept fixed and R decreases according to the water removal, and b) R is fixed and η decreases. The PBG evolution shows clearly different features for both limits. In the limit (a), only R decreases upon water loss, so only n_v varies (decreases) while d_{111} and f remain unchanged, as in the close-packing case. The predicted PBG blueshift (29 nm) nearly matches the overall experimental change but the trend of FWHM still disagrees. By contrast, in the limit (b), the decrease of η implies the contraction of the opal structure, which leads not only to an n_v decrease but also to both a d_{111} decrease and an f increase. With these new contributions, λ_{Bragg} is predicted to further blueshift and, remarkably, FWHM is now expected to steadily decrease, like the experimental trend. That the theoretical changes in limit (b) clearly exceed those measured just indicates that such extreme is not realistic. In turn, it is expected that actually all d, η, and R vary simultaneously.

These calculations confirm the qualitative discussion made in the previous section. Moreover, it becomes evident that only the nonclose fcc packing can account for the experimental results, in particular for the behavior of the Bragg peak width. As shown, the compaction of the opal structure due to water removal enables the bandgap narrowing in spite of the increase of the refractive index contrast. Thus, the presence of water between contiguous spheres (forming necks) rather than in the voids facilitates an overall FWHM decrease. The exact parameters for each water content are next found by fitting the experimental data.

2.4. Calculation of Water Distribution in the Opal

As discussed, the opal is in general fully described by three unknown parameters (d, η, and R), which are interrelated through the amount of water. The latter is known from TGA for each heating temperature, so that the problem is reduced to find two unknowns. To find them, we adjust two experimental data for each water content (we use λ_{Bragg} and FWHM from Figure 3) by performing a least-squares fitting using an iterative process (see Experimental Section). The resulting best fit (black lines in Figure 3) shows perfect agreement with the measured FWHM over the whole experiment. Also a complete accord with the experimental λ_{Bragg} is possible up to ~4.5 wt.% of water ($T \approx 65$ °C). For higher T, the model cannot fully reproduce the measurement but the attained agreement is fairly good and the error is always less than 10% of the changes (about 2% in average). In particular, the worst fit is obtained for 80–160 °C, where the experimental FWHM shows a maximum (see Figure 2c).

From this fitting we obtain, for every experimental point, a set of parameters evolving with the removal of the water, which describes the water distribution in the opal and its progress upon heating (**Figure 4**). At RT, the water is disposed between necks with $\eta = 16$ nm and $R = 67$ nm and the film on the spheres with $d \sim 7$ nm (see inset in Figure 4a). These values correspond to a ratio $\rho \sim 0.5$, so water is rather homogeneously distributed in the opal at RT. Upon water desorption, the parameters behavior shows two marked regimes (depicted in Figure 4 with a dashed line). In the first stage, up to 4.4 wt.% ($T \sim 65$ °C), d quickly vanishes (so ρ increases towards 1). Simultaneously, η steadily decreases to one-fourth of its initial value ($\eta = 4$ nm at $T \sim 65$ °C) while R remains constant, i.e., necks become significantly narrower. In the second stage, at higher T, water remains completely eliminated from the voids ($d \approx 0$) while η keeps decreasing at the same pace until almost vanishing ($\eta \sim 1$ nm at 285 °C) and R also begins to diminish but less markedly than η. Thus, at high temperatures silica spheres are practically in contact

NANO MICRO small

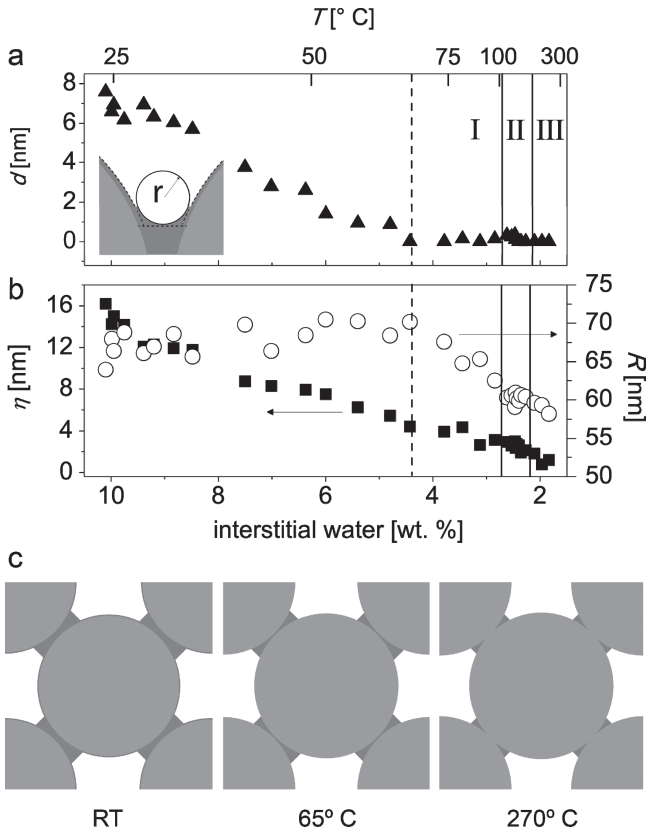

Figure 4. Evolution of the model parameters upon water removal as obtained from fitting of experimental data (a,b). c) Side view of the fcc unit cell with the obtained water distribution in the opal at RT, 65 °C, and 285 °C with lattice parameters of 287, 277, and 274 nm, respectively (proportions are maintained). Inset in (a): geometrical estimation of the corresponding meniscus at RT (see text), where water neck and films assumed in the model are depicted by dashed lines.

and the remaining water forms an annulus around the contact points.

The results imply a nonclose-packed fcc arrangement of the spheres (Figure 4c) and experimentally confirm evidences in this direction. At RT, water necks separate the spheres about 16 nm, which remarkably represents a 5% of the spheres size and leads to an actual filling fraction of 0.64. These values are in good agreement with previous estimates ($f = 0.60$ in reference [10] and 0.61 in reference [18]). Studies on opals formed by much less hydrophilic spheres than as-grown silica ones, made, e.g., by polymer[16,19] or calcined silica,[16] report filling fractions at RT significantly larger ($f \approx 0.72$), which strongly suggests that the adsorption of water on the spheres surface is, in fact, responsible for the nonclose-packed arrangement. The silica opal significantly contracts by warming up only ~40 °C and adopts a near close-packed structure at $T > 200$ °C, although water is still present (Figure 4b). Regarding the desorption behavior, we obtain more pronounced dehydration in the opal voids and only water located in the necks persist at T as low as 65 °C. This is in agreement with the general behavior of dehydration in porous systems, where the water placed in crevices requires higher temperatures to be removed.[12] Note, however, that some water can be transfused by capillarity from the voids to the necks. This agrees with the fact that R begins to decrease only when the water has been completely removed from the voids (at $T \sim 65$ °C). From data in Figure 4, regions I–III (observed in TGA) has no obvious influence on the evolution of the water distribution. This point is unclear and requires further investigation. Regarding the dimensions of the water necks (R between 55 and 70 nm), they are significantly smaller than both types of voids in the opal, tetrahedral on octahedral. Moreover, the maximum R is still far from blocking the internal windows linking the opal voids. Otherwise, having more adsorbed water would alter the distribution pattern throughout the opal, as the voids would be no more interconnected (this occurs, in fact, during conformal growth in opals by chemical vapor deposition, which is therefore limited to a maximum infiltration of 86% of the voids[20]). That is, given that the volume occupied by the adsorbed water is relatively small, the water distribution between and on the individual spheres is probably not affected by the general opal structure.

Finally, it is interesting to examine more realistic water necks by considering, at the contact regions, the formation of spherical concave menisci compatible with the parameters values we obtained for each experimental point. We geometrically estimate the corresponding meniscus radius (r) by adjusting a sphere to be tangential to both the water neck and the film (we find $r = 22$ nm at RT, see inset in Figure 4a). It is important to note that the water volume resulting from this construct is only slightly larger than that considered in our model and we confirmed that it has negligible influence on the results. For the sake of comparison, the classical capillary theory[12] predicts, according to the equilibrium Kelvin equation, a meniscus radius of $r \approx 1.4$ nm at RT and humidity of 40%, which is one order of magnitude smaller than our estimation. On the other hand, the film thickness we find at RT ($d \sim 7$ nm) agrees well with values reported for tightly bound surface layers of water on silica (~4 nm).[21] In any case it is known that the classical capillary theory provides an oversimplified description of water condensation under a number of conditions. In particular, condensation in nanometric systems is a complex issue and its full description is still an open question,[11,22] which may involve aspects like electrostatic and van der Waals forces (DLVO theory), surface roughness, interfacial energy, etc. Our study demonstrates that a silica opal offers an ideal system to obtain, from its optical properties, valuable information about water-related phenomena in nanometric structures.

3. Conclusion

Using a simple model, we fully describe the distribution of interstitial water in an opal (only assuming fcc packing of spheres with a given size) by just three geometric parameters. They are obtained from three experimental, easy to measure values: on the one hand, the amount of water at each temperature (calculated from TGA) and, on the other hand, both the position and width of the Bragg peak (from opal reflection spectrum). We find that the distribution pattern of water greatly affects the optical properties of the opal. This allows

the study of water desorption by directly monitoring the opal PBG. Thus, we perform heating experiments in a silica opal and measure in situ the changes in the reflection spectrum. Experimental data are well fitted by our model without adjusting any further opal parameter. From the measurements we obtain the water distribution for each temperature (i.e., for each water content) and, thus, the progression of water removal.

We quantitatively show that the opal properties are incompatible with an ideal close-packed fcc structure. Recently, deviations from ideal fcc packing have also been investigated in both polymer[14,23,24] and silica[14] opals. In these studies, the presence of water was not considered and distorted close-packed fcc structures, assuming spheres contraction as large as 5%, were necessary to explain the discrepancies. By contrast, in our approach the presence of water between spheres of a silica opal naturally leads to a nondistorted nonclose-packed fcc structure that accounts for the opal properties (and its behavior upon dehydration) without further assumptions. In particular, the unexpected observation of PBG narrowing is explained by the contraction of the opal structure due to water removal, in spite of the increase of the refractive index contrast. According to our model, we find a filling fraction at RT as low as 0.64. Further, water desorption is more pronounced in the opal voids than between spheres, so that water exclusively resides in the necks at temperatures above 65 °C. Even at 285 °C some adsorbed water remains in the opal, concentrated at the interstices formed by adjacent spheres. Interestingly, the separation between spheres is accurately tuned with the temperature from 16 to about 0 nm, which might offer a simple tool for precise control of particle motions at the nanometer scale.

Finally, the optical properties of a silica opal offer an ideal tool to investigate liquid/solid interface phenomena in nano- to micrometric structures using a simple optical characterization. The well-defined morphology of opaline structures (porosity, pore size and form, and pore space connectivity) is further advantageous to systematize such studies. Thus, our novel approach may have implications not only for colloidal science (applied to generic humid granular media) but also for many fields in which capillary/adhesion issues play a role, like scanning microscopy,[25] photonic applications,[26] and general wetting research.[27]

4. Experimental Section

Opal Fabrication: Artificial opal templates are prepared from a dilute ethanol colloidal suspension of monosized (polydisperity of ≈3%) 335 nm silica spheres synthesized at room temperature by the Stöber–Fink–Bohn procedure,[28] following the vertical deposition method[29] in controlled temperature and humidity conditions using a Binder KBF Constant Climate Chamber (at 50 °C and 60% relative humidity). For this purpose, both glass substrate and vial are hydrophilized by immersion in HCl during 24 h. The vial is filled with 5 mL of colloidal suspension with a concentration of 1.9% w/w, closed with a cap and thermalized, together with the substrate, in the climate chamber for 20 min. Afterwards, the substrate is introduced with an angle of 0–5° from vertical into the open vial. After solvent evaporation, a solid fcc structure of silica spheres is obtained. Although the growth takes only some hours, the opal is left inside the chamber for 72 h to eliminate residual solvent. The resulting opals, with size of ~1 cm^2, are formed by ~35 monolayers and their quality is checked by optical characterization and scanning electron microscopy. Note that the thermalization step greatly enhances the samples quality.

Thermal Gravimetric Analysis: TGA was performed by a Mettler Toledo TGA/DSC 1 on a silica opal detached from the glass substrate. The sample was heated in air up to 850 °C at a heating rate of 10 °C min^{-1}.

Reflection Spectra: The opal PBG was characterized by measuring reflection spectra with an Ocean Optics 2000+ spectrometer using white light (halogen lamp Osram HLX 64623). The opal was set on a hot plate for controlled heating while reflection spectra were simultaneously measured (Figure 2a, inset). The hot plate temperature was varied between RT (22 °C in our laboratory) and 285 °C. Before every measurement, T was maintained for 30 min in order to ensure thermal equilibrium, although PBG changes were observable right after T was changed.

PBG Properties and MPB Calculations: Opal properties can be inferred from the form and position of the PBG. In a first approximation, Bragg's law describes the position of the Bragg peak (the lowest energy PBG, associated to the diffraction at the (111) family of planes: see Figure 2a, inset), which is given at normal incidence by

$$\begin{aligned} \lambda_{\text{Bragg}} &= 2d_{111}\, n_{\text{eff}} \\ n_{\text{eff}} &= \sqrt{f n_{\text{p}}^2 + (1-f) n_{\text{v}}^2} \end{aligned} \tag{1}$$

where n_{p} is the refractive index of the spheres and the lattice parameter d_{111} is referred to the spacing of the (111) planes. In ideal (close-packed) fcc structures, $f = 0.74$ and $d_{111} = (2/3)^{1/2}\, D$. n_{p} is 1.43 (refractive index of silica at ~700 nm), and n_{v} depends on the medium filling the opal voids, in our case, air and water (with a filling fraction f') and it is given by

$$n_{\text{v}} = \sqrt{f' n_{\text{water}}^2 + (1-f') n_{\text{air}}^2} \tag{2}$$

where n_{water} and n_{air} are the refractive indices of water (1.33) and air (1.0), respectively. Bragg's law does not offer any description of the PBG width.

Calculations of the PBG position and width were accomplished using the MPB software,[30] which allows the simulation of inhomogeneous distribution patterns of the water inside the opal. MPB computations assume infinite media and they can significantly differ from measurements in real systems due to finite size effects.[31] In silica opals, finite size effects can be disregarded above 10–15 layers.[32] This allows direct comparison between measurements in our 35-layers opals and MPB calculations.

Calculation of the Fitting Parameters: We choose both the thickness d and the neck width η as the two unknowns to be found. For each T (i.e., for each amount of water), we resolve d (T) and η (T) by fitting to both experimental λ_{Bragg} (T) and *FWHM* (T) in Figure 3 using the least-squares method. Formally, we perform iterative MPB calculations to obtain $h_{1,2}{}^{\text{MPB}}(d\,(T), \eta\,(T))$, with $h_1 = \lambda_{\text{Bragg}}$ and $h_2 =$ FWHM, varying d and η in order to minimize the fit error function for each T:

NANO MICRO small

$$\chi\left(\mathrm{d}(T),\eta(T)\right)^2 = \sum_{i=1}^{2}\left(h_i\left(\mathrm{d}(T),\eta(T)\right) - h_i^{\mathrm{MPB}}\left(\mathrm{d}(T),\eta(T)\right)\right)^2$$

where the superscript MPB refers to the calculated values. As a general rule, the resultant values d and η minimizing χ^2 lead to vanishing error in FWHM. This occurs because $\mathrm{FWHM}^{\mathrm{MPB}}$ is more sensitive to changes in d and η than $\lambda_{\mathrm{Bragg}}{}^{\mathrm{MPB}}$. Consequently, the best fit yields complete agreement with the experimental bandgap width while the error in the Bragg position is the minimum (Figure 3).

Acknowledgements

FGG was supported by the JAE Postdoctoral Program from the CSIC. This work was partially supported by EU FP7 NoE Nanophotonics4Energy grant No. 248855; the Spanish MICINN CSD2007–0046 (Nanolight.es), MAT2009–07841 (GLUSFA) and Comunidad de Madrid S2009/MAT-1756 (PHAMA) projects.

[1] J. F. Galisteo-López, M. Ibisate, R. Sapienza, L. S. Froufe-Pérez, A. Blanco, C. López, *Adv. Mater.* **2011**, *23*, 30.
[2] H. Miguez, C. López, F. Meseguer, A. Blanco, L. Vázquez, R. Mayoral, M. Ocaña, V. Fornés, A. Mifsud, *Appl. Phys. Lett.* **1997**, *71*, 1148.
[3] H. Miguez, F. Meseguer, C. López, A. Blanco, J. S. Moya, J. Requena, A. Mifsud, V. Fornés, *Adv. Mater.* **1998**, **10**, 480.
[4] F. Garcia-Santamaria, H. Miguez, M. Ibisate, F. Meseguer, C. Lopez, *Langmuir* **2002**, *18*, 1942.
[5] A. A. Chabanov, Y. Jun, D. J. Norris, *Appl. Phys. Lett.* **2004**, *84*, 3573.
[6] Y. Yamada, T. Nakamura, M. Ishii, K. Yano, *Langmuir* **2006**, *22*, 2444.
[7] G. Kresse, J. Furthmuller, *Phys. Rev. B* **1996**, *54*, 11169.
[8] W. Kohn, N. Rostoker, *Phys. Rev. B* **1954**, *94*, 1111.
[9] I. I. Tarhan, G. H. Watson, *Phys. Rev. B* **1996**, *54*, 7593.
[10] M. D. Sacks, T.-Y. Tseng, *J. Am. Ceram. Soc.* **1984**, *67*, 526.
[11] *Colloidal Silica: Fundamentals and Applications* (Eds: H. E. Bergna, W. O. Roberts), CRC Press, Boca Raton **2006**.
[12] J. N. Israelachvili, *Intermolecular and Surface Forces*, 2nd ed., Academic Press, London **1992**.
[13] G. M. S. El Shafei, in *Adsorption on Silica Surfaces* (Ed: E. Papirer), Marcel Dekker Inc., New York **2000**, Ch. 3.
[14] G. Lozano, L. A. Dorado, D. Schinca, R. A. Depine, H. Míguez, *Langmuir* **2009**, *25*, 1 2860.
[15] I. I. Tarhan, G. H. Watson, *Phys. Rev. B* **1996**, *54*, 7593.
[16] F. Garcia-Santamaria, P. V. Braun, *Appl. Phys. Lett.* **2007**, *90*, 241905.
[17] One could try a better fitting by choosing the spheres diameter within its nominal error ($D = 335 \pm 10$ nm). Indeed, the calculation matches the experimental λ_{Bragg} for $D = 328.6$ nm (in the subcase of $R = 0$) but similar mismatch with FWHM is obtained (at RT, 13 nm instead of 14 nm). Moreover, the behavior upon water desorption is identical.
[18] Míguez, H. Ph.D. Thesis, Universidad Autónoma de Madrid, Madrid, July 2000.
[19] Y. Yin, Z.-Y. Li, Y. Xia, *Langmuir* **2003**, *19*, 622.
[20] H. Miguez, N. Tetreault, B. Hatton, S. M. Yang, D. Perovic, G. A. Ozin, *Chem. Commun.* **2002**, *22*, 2736.
[21] A. Grabbe, R. G. Horn, *J. Colloid Interface Sci.* **1993**, *157*, 375.
[22] N. Maeda, J. N. Israelachvili, M. M. Kohonen, *Proc. Natl. Acad. Sci. USA* **2003**, *100*, 803.
[23] J. F. Galisteo-López, M. Galli, A. Balestreri, M. Patrini, L. C. Andreani, C. López, *Opt. Express* **2007**, *15*, 15342.
[24] I. Popa, F. Marlow, *ChemPhysChem* **2008**, *9*, 1541.
[25] M. Köber, E. Sahagún, P. García-Mochales, F. Briones, M. Luna, J. J. Sáenz, *Small* **2010**, *6*, 2725.
[26] P. Barthelemy, M. Ghulinyan, Z. Gaburro, C. Toninelli, L. Pavesi, D. S. Wiersma, *Nat. Photon.* **2007**, *1*, 172.
[27] A. Méndez-Vilas, A. B. Jódar-Reyes, M. L. González-Martín, *Small* **2009**, *5*, 1366.
[28] W. Stöber, A. Fink, E. Bohn, *J. Colloid Interface Sci.* **1968**, *26*, 62.
[29] P. Jiang, J. F. Bertone, K. S. Hwang, V. L. Colvin, *Chem. Mater.* **1999**, *11*, 2132.
[30] MIT Photonic Bands (MPB) software. S. G. Johnson, J. D. Joannopoulos, *Opt. Express* **2001**, *8*, 173.
[31] J. F. Galisteo-Lopez, E. Palacios-Lidon, E. Castillo-Martinez, C. Lopez, *Phys. Rev. B* **2003**, *68*, 115109.
[32] J. F. Bertone, P. Jiang, K. S. Hwang, D. M. Mittleman, V. L. Colvin, *Phys. Rev. Lett.* **1999**, *83*, 300.

Received: January 26, 2011
Revised: March 1, 2011
Published online: May 12, 2011

